# Hydrogen storage for off-grid power supply based on solar PV and electrochemical reforming of ethanol-water solutions

F. Gutiérrez-Martín[a], A.B. Calcerrada[b], A. de Lucas-Consuegra[b], F. Dorado[b]

[a] *ETSIDI, Universidad Politécnica de Madrid, Rda.Valencia 3, 28012 Madrid, Spain*

*fernando.gutierrez@upm.es*

[b] *Dept. Ingeniería Química, Univ. Castilla-La Mancha, 13071 Ciudad Real, Spain*

**Abstract**

The hybridization of hydrogen and solar energy technologies is an interesting option to satisfy power demands in locations that are isolated from the electric grid. The main advantage of the photovoltaic (PV)-$H_2$ hybrid system is the possibility of power storage by means of an electrolyzer (EL), which transforms the electricity into hydrogen ($H_2$) that can be used in fuel cells.

The work described here concerns a methodology to design PV-$H_2$ hybrid systems that considers the weather data and the electrical variables of the components to perform energy balances and to assess the system in terms of the load requirements, the levels of energy stored and the resulting costs. The results show that if PV-EL coupling can be improved, the solar field is smaller but the size of EL becomes much larger. Therefore, it is not advantageous to operate close to the maximum power points (MPPs) of the PV arrays (even if this leads to better energy efficiency). Two electrolytic systems (water splitting and ethanol electrochemical reforming) were studied in an attempt to find the best trade-off between the size and voltages of ELs. Ethanol reforming reduced the energy requirement of electrolysis at the expense of reagent consumption and lower current density values. If an inexpensive substrate is utilized, the analysis indicates the cost reduction of the organic electrolyzer (43%) to match the same annual costs as water electrolyzers. The energy supplied by this system cost 0.28 €/kWh (i.e., roughly the same as power prices paid by domestic customers in Spain), but it has the merit of being autonomous and hydrogen has the capacity for seasonal storage – thus avoiding electrification constraints in off-grid locations and limitations of short-term storages. Then, PV-$H_2$ systems can play a role in implementing distributed energy supplies that require compact, long life and low maintenance devices.

Keywords: Hybrid power system; PV energy; Hydrogen; Electrolysis; Electrochemical reforming.

**Nomenclature**

| | |
|---|---|
| PV | Photovoltaic component |
| EL | Electrolyzer component |
| FC | Fuel-cell component |
| C | Power demand, W or kWh/d |
| f | Sizing factor of the energy system |
| t | time, h/day |
| G | Solar radiation, $W/m^2$ |
| T | PV module temperature, °C or K |
| $T_a$ | Ambient temperature, °C |
| NOCT | Nominal operation cell temperature, °C |
| I | Current, A or kC/d |
| V | Voltage, V |
| P | Power, W |
| $I_{MPP}$ | PV current at maximum power point (MPP), A |
| $V_{MPP}$ | PV voltage at maximum power point (MPP), V |
| $I_{sc}$ | PV short-circuit current, A |
| $\mu_{Isc}$ | Temperature coefficient of $I_{sc}$, A/°C |
| $V_{oc}$ | PV open circuit voltage, V |
| $\mu_{Voc}$ | Temperature coefficient of $V_{oc}$, V/°C |
| $I_o$ | PV cell reverse saturation current |
| $R_s$ | PV cell series resistance, Ω |
| r | Parameters (subscript) at standard test conditions (STC) |
| $E_g$ | Energy gap of the PV cell, eV |
| $N_{PV}$ | Number of PV modules or PV cells in series (s) or parallel (p) |
| J | Current density at the EL, $A/cm^2$ |
| $E_o$ | Thermodynamic parameter of EL, V |
| K | Kinetic parameter of EL, $\Omega^{-1}\ cm^{-2}$ |
| R | Ohmic parameter of EL, $\Omega \cdot cm^2$ |
| $N_{EL}$ | Number of EL cells in series |
| S | Electrode area per PV module (EL), PV array (CEL) or total (NEL), $cm^2$ or $m^2$ |
| $\eta_{EL}$ | Efficiency of EL due to balance-of-plant (BOP) and current losses, 90% |
| $\mathfrak{F}$ | Faraday constant, 96.5 $kC/g_{H2}$ |
| $Q_H$ | Hydrogen production, g/h or g/d |
| $C_e$ | Specific energy yield of EL, $kWh/kg_{H2}$ |
| $\eta_e$ | EL efficiency based on the lower heating value of $H_2$ (LHV: 33.554 kWh/kg), % |
| SOC | Cumulative hydrogen stored (LHV), W or kWh/d |
| $\eta_{FC}$ | Fuel cell efficiency (LHV), 60% |
| $C_a$ | Annual costs, €/a |

## 1. Introduction

The development of integrated energy efficient systems built with renewable sources and hydrogen technologies can play an important role in reducing the energy use from fossil fuels and pollution emissions. Moreover, the diffuse structures of residential energy demand may be appropriate to implement distributed generation systems from local renewable energies, where the sun is a preferred resource because of its ready availability. However, the intermittent nature of solar radiation makes it challenging to generate reliable energy with photovoltaic (PV) modules alone. Thus, the continuous supply of power to off-grid electricity consumers depends on energy storage, where chemical carriers such as hydrogen ($H_2$) have the advantage of not losing their energy content while not in use.

The overall configuration of a PV-$H_2$ hybrid system for a grid of an independent house is shown in Fig. 1. The main advantage of the hybrid system compared to a separate PV array is the possibility of surplus energy storage by transforming it into $H_2$ that can be used in fuel cells (FCs): if the power generated by the primary system (PV) is higher than the electrical demand, the surplus energy is used in an electrolyzer to produce $H_2$; if the PV is not sufficient to meet the loading, the energy required is provided from the $H_2$ storage and is used in the FCs.

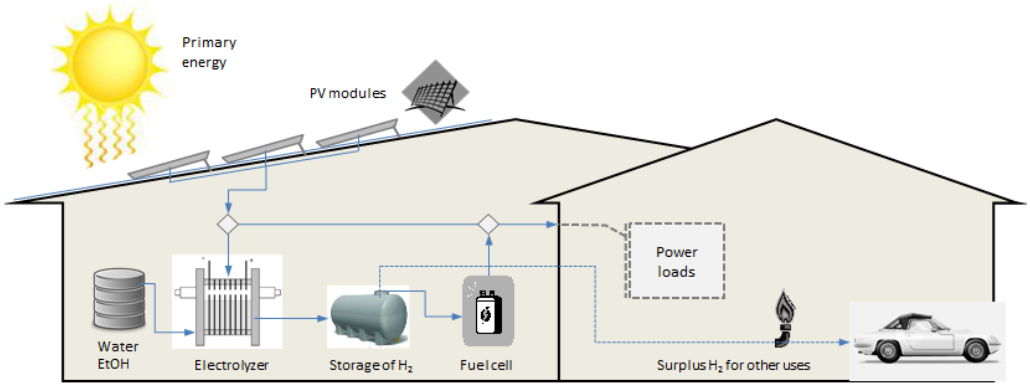


Fig. 1. Hybrid system for off-grid power supply based on solar PV and hydrogen storage

Thus, the hybrid system consists of PV modules coupled to an electrolyzer (EL) and FCs that must meet certain requirements:

- The system should supply a minimum voltage to the electrolyzer to carry out the splitting of water (theoretically 1.23 V and experimentally around 1.4–2 V).
- Each subsystem (PV and EL) should work near to their maximum power points (MPP) at a given irradiance and temperature in order to maximize efficiency.
- The nominal capacity of each subsystem should be carefully selected to satisfy the electricity demands but without oversizing the system.
- The system should contain a minimum of auxiliary devices (e.g., power conditioning and others) so that the global efficiency and costs are optimized.

Numerous hybrid systems based on renewable energy and $H_2$ for single buildings have been discussed previously, including the solar inputs and load dynamics, the trade-offs between primary energy rates, load profiles and storage capacity, the PV-EL coupling without MPP trackers (MPPT) and power converters, the operation and efficiency of EL, and the cost reductions required to compete with conventional energy systems [1-13].

Several studies have been carried out in an attempt to find the size and operation of directly coupled PV-EL systems to optimize the energy transfer and $H_2$ production, including the simulation of realistic hybrid systems. For a directly connected system, the EL operates at the intersection points between the PV output and EL input curves for different irradiance levels, although there are no definitive concepts to guide the method for the connection of PV and EL without the use of MPPT techniques [14-20].

The work described here concerns a comprehensive model to size, analyze and assess PV-$H_2$ systems. The model considers the weather data and the electrical variables of the components to perform rigorous energy balances and calculate the efficacy of the system in terms of the levels of energy stored and the loading requirements.

The hybrid system design is dependent on the performance of individual components, which were modeled first. The combination of these components was then evaluated to meet the demand reliably. As far as the PV-EL analysis was limited in other studies to simpler systems in which the entire PV output is fed into the EL at all times, we attempt to find the optimal arrangement in the most desirable configuration shown in Fig. 1.

The most common solar cells are made from doped silicon films and they are classified as mono- and polycrystalline. PV modules are arrangements of cells with different sizes in such a way that they allow the generation of electrical power to operate an EL. The hybrid systems were studied without batteries or complex power electronics, showing that a good knowledge of PV and EL behavior allows the optimization of stand-alone energy systems that fulfill the electricity needs in full operation over time. The primary energy source is the solar radiation to the PV array formed by modules (106 W each) of monocrystalline silicon (c-Si) interconnected in a configuration at 34.8 $V_{DC}$. These are the most suitable modules for the installation of solar trackers and they are also more efficient than polycrystalline solar cells, with better results obtained in cold climates.

The hydrogen subsystem consists of a proton exchange membrane (PEM) electrolyzer, a tank for $H_2$ storage and a fuel cell (PEMFC). PEM-type electrolyzers offer advantages such as high $H_2$ purity, small size, stable electrolyte and lower energy consumption without the requirement to maintain a voltage, unlike in alkaline cells. Two processes (conventional water splitting and ethanol reforming) are compared and this represents another novel aspect of this work in an effort to find the best compromise between minimum voltage and size of electrolyzers. The electro-oxidation of organic solutions is a recent alternative to decrease the energy demand in electrolytic production of $H_2$, as the energy contained in these compounds supplies a part of the power requirements, thus enabling high current density at low anode potentials (<1.3 V) [21-23].

Finally, the $H_2$ is stored in a tank and transformed into electrical energy in a PEMFC with efficiencies up to 60% and only heat and water are produced as byproducts.

The technology, manufacture and marketing of many of these components are in early stages of development and, as a consequence, the costs of the hybrid systems are still very uncertain. The economics of PV-$H_2$ systems will be determined by the cost of the components, their capacity factors and their efficiency. One must also take into account competitive technologies and therefore the main contribution of an economic analysis is to establish a baseline of current technologies to meet residential loads, i.e., the costs and lifetimes of PV, EL and FC for comparison with current energy alternatives (electricity and fuels) and other storage methods.

Bearing the above objectives and considerations in mind, the manuscript is organized as follows:

- Section 2 covers the primary energy of the system (i.e., the solar radiation converted into electrical energy), in which the PV cells are simulated by means of power curves at different radiation levels and temperatures in the solar modules.

- In Section 3 the electrolytic processes are described by means of their power curves, which were obtained from research into conventional and ethanol electrolyzers.

- In Section 4 the hybrid system is fully modelled by the solar inputs, the PV array and its coupling to the electrolyzers, the $H_2$ production and the FC to meet the power loads.

- In Section 5 the results of simulations are discussed, including the optimal design and sensitivity analysis in order to compare the systems studied with other alternatives.

- Finally, the main findings and conclusions of this study are summarized in Section 6.

## 2. Solar radiation and characterization of PV cells

### 2.1. Primary energy

The primary energy source is the solar radiation available at the site which is converted into electrical energy with a set of PV cells, where the electricity generation depends on the insolation level, temperature and properties of the cells.

The radiation (G) and temperature (T) profiles in the solar-PV modules can be simulated with the following expressions:

$$G = \tfrac{1}{2} G_m [1 - \cos(2\pi t/\Delta t)] \quad (1a) \qquad T = T_a + 10^3 \cdot G \cdot (NOCT - 20)/800 \quad (1b)$$

where $G_m$ (W/m$^2$) is the maximum solar power density, t is the time between sunrise ($t_1$) and sunset ($t_2$) ($\Delta t = t_2 - t_1$) and NOCT is a parameter of PV cells; e.g., Fig. 2 shows the daily radiation profile and cell temperature for $G_m$ = 1000 W/m$^2$, with dawn and sunset at 8 and 18 h, respectively, NOCT 47°C and ambient temperature: $T_a = 5 + 15 \cdot G$.

This profile depends on climatic conditions, geographic latitude, season of the year and inclination of the modules, but this can be considered as a base day for the purposes of preliminary design of facilities; hence, calculations can be extended to annual periods with full-year-daily-average data or measurements from local meteorological stations.

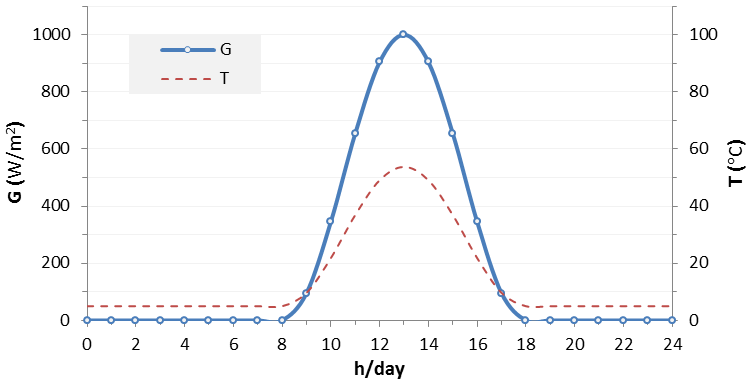


Fig. 2. Daily profile of solar radiation and PV cell temperatures

## 2.2. Photovoltaic (PV) cells

The energy production of the solar array is determined by the current-voltage curves of the PV cells. These curves depend on the radiation levels (G), the temperatures (T) and parameters such as the short-circuit current ($I_{sc,r}$, $\mu_{Isc}$), the open voltage ($V_{oc,r}$, $\mu_{Voc}$), the intensity and voltage at the maximum power point ($I_{MPP,r}$, $V_{MPP,r}$), the energy gap ($E_g$) and the number of cells in series/parallel ($N_s$, $N_p$).

The problem of finding model circuit parameters for PV cells is crucial for performance evaluation, control, efficiency computations and MPP tracking of solar PV systems [24]. The model presented by Duffie & Beckmann [25], which is the most widely cited in the literature [26], was selected for PV characterization in this study (eq. 2), along with the relations to work out the parameters [27] in Table 1 and the information datasheet for the PV (c-Si) technology shown in Fig. 3.

$$V = \alpha \cdot \ln[(I_{sc} - I)/I_o + 1] - I \cdot R_{s,r} \qquad (2)$$

Table 1. Relations for the PV model at standard test conditions (STC) and variations from STC

| **Parameters at STC** | **Variation from STC** |
|---|---|
| $\alpha_r = (\mu_{Voc} \cdot T_r - V_{OC,r} + E_g N_s)/(\mu_{Isc} T_r/I_{SC,r} - 3)$ | $\alpha = \alpha_r \cdot T/T_r$ |
| $I_{o,r} = I_{SC,r} \exp[-V_{OC,r}/\alpha_r]$ | $I_o = I_{o,r} (T/T_r)^3 \exp[(1 - T_r/T) \cdot E_g N_s/\alpha]$ |
| $R_{s,r} = [\alpha_r \ln(1 - I_{MPP,r}/I_{SC,r}) - V_{MPP,r} + V_{OC,r}]/I_{MPP,r}$ | $I_{sc} = G/G_r \cdot [I_{SC,r} + \mu_{Isc}(T - T_r)]$ |

The power vs. voltage characteristics of the PV cell show a maximum and this depends on the cell temperature and insolation. The current-voltage (I-V) curves are shown in Fig. 3 along with MPP ($I_{MPP}$, $V_{MPP}$) estimations for different values of solar irradiance and temperatures, which correspond to the daily profile outlined in section 2.1.

The output of the hybrid system is then determined from the I-V curves, which represent the PV and EL operational characteristics for a given set of conditions. However, even if the PV-EL were perfectly coupled for one set of conditions that would not necessarily be applicable to another depending on the dynamics of the PV and EL: this is the case in following sections, where they are initially well coupled for the sunny conditions ($G_m$).

| **Manufacturer data** | |
|---|---|
| $V_{MPP,r}$ (V) | 34.8 |
| $I_{MPP,r}$ (A) | 3.05 |
| $I_{SC,r}$ (A) | 3.27 |
| $V_{OC,r}$ (V) | 43.2 |
| $\mu_{Isc}$ (A/K) | 1.8e-4 |
| $\mu_{Voc}$ (V/K) | -0.16 |
| $E_g$ (eV) | 1.12 |
| $N_s$, $N_p$ | 72, 1 |
| NOCT (°C) | 47 |

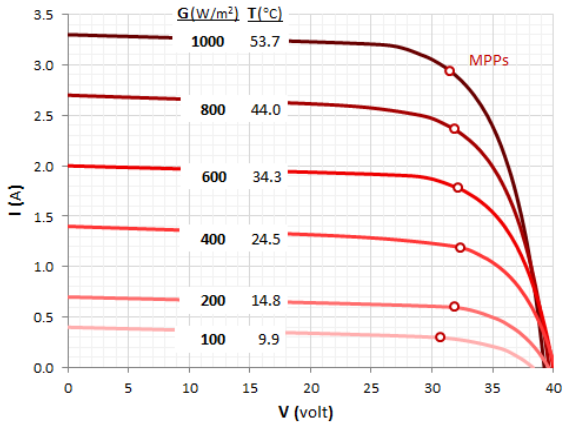


Fig. 3. I-V curves corresponding to the datasheet for PV modules at STC ($G_r$ : 1 kW/m$^2$, $T_r$ : 25°C); NOCT is at 800 W/m$^2$, 20°C and wind speed 1 m/s

## 3. Investigation and characterization of the electrolyzers

The electrolyzer receives the electrical energy from the PV modules and the production of hydrogen will be determined by the properties of these components. Therefore, the I-V behavior of the EL must be known so that both subsystems are coupled as closely as possible to the maximum PV power (MPP) through an optimum array arrangement.

For this purpose, we start from the characteristic curves of two PEM-type electrolytic systems (with water and ethanol) that fit a concise model of three parameters (eq. 3), where the current density is the electrical intensity per unit of electrode area (J = I/S).

$$V = [J + 2K\,(J \cdot R + E_o) + (J^2 + 4K \cdot E_o\, J)^{1/2}] / 2K \qquad (3)$$

This model describes electrolysis by means of three parameters: the thermodynamic voltage ($E_o$), which is related to the water dissociation potential, the kinetic parameter (K), which reflects the overall electrochemical kinetic effect of both electrodes, and the ohmic parameter (R), which accounts for the total electrical resistance of the cell [28].

### 3.1. Water electrolysis

The characteristics of a conventional water electrolyzer are based on the research of Millet et al. [29] on PEM cells with low resistance and high operating current density at a temperature of 90°C. In this case, when platinum is used in the cathode and iridium is employed in the anode, the water dissociation potential is 1.40 V, the cell resistance is 0.15 $\Omega \cdot cm^2$ and the kinetic parameter is 27.8 $\Omega^{-1}cm^{-2}$ (Fig. 4a).

### 3.2. Ethanol electrolysis

The electrochemical reforming of ethanol (EtOH) for hydrogen production in a PEM cell was reported by De Lucas-Consuegra et al. [30]. Moreover, these authors prepared a novel Pd anode with high electro-catalytic activity (up to 700 mA/$cm^2$) to produce very pure faradic $H_2$ with a low energy demand. The most effective electrolyte in the fuel solution was KOH and an increase in temperature enhanced activity up to 90°C [31]. The curves with 2 M EtOH and 1 M KOH at 80°C were chosen for this work, showing an electrochemical potential of only 0.40 V, but a higher cell resistance (0.30 $\Omega \cdot cm^2$) and much lower kinetic activity (1.2 $\Omega^{-1}cm^{-2}$) than conventional water electrolysis (Fig. 4b).

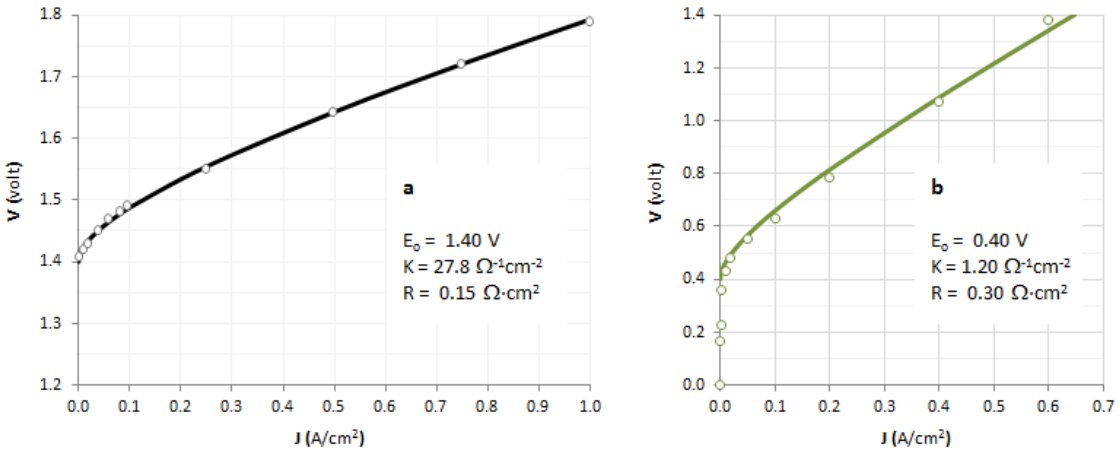


Fig. 4. Polarization curves for PEM water electrolysis (a) and electrochemical reforming (b)

## 4. Setting the electrical loads and modeling the hybrid system

The power loads and their typical hourly profiles were estimated for the whole day – as shown in the case outlined below – before proceeding to model the hybrid systems, where calculations are based on the same solar and temperature profiles, to perform a comparative design of the equipment with an optimal size and load coverage.

### 4.1. Electrical loads

Representative electric devices within a typical residence were considered to estimate the loads (including power and hours of daily operation): five luminaires (20 W, 5 h), a washing machine (600 W, 1 h), a television (120 W, 2 h), a stereo (50 W, 1 h), a computer (115 W, 3 h), a climatizer (110 W, 10 h) and a refrigerator (200 W, 24 h), amounting to an electricity demand of C = 7.635 kWh/day.

On the basis of the above appliances a distribution of the loads was prepared according to Table 2. These loads occur mainly in the morning and evening when there is low solar availability; most of the PV output is unused during midday and this time offset between supply and demand leads to only 36.5% (2.790 kWh) of the residential load demand possibly being met directly by the PV, with 63.5% (4.845 kWh) of the demand requiring the hydrogen storage devices: i.e., the $H_2$ that has been produced by the electrolyzer and stored in a gas cylinder is used in the fuel cell to meet the simulated residential load dynamics shown in the last column of Table 2.

Table 2. Electrical loadings of different appliances and services for a representative house/day

| Time (h) | Lamps | Washer | TV | Stereo | PC | Climatizer | Fridge | Total (W) |
|---|---|---|---|---|---|---|---|---|
| 0:00 | | | | | | | 200 | **200** |
| 1:00 | | | | | | | 200 | **200** |
| 2:00 | | | | | | | 200 | **200** |
| 3:00 | | | | | | | 200 | **200** |
| 4:00 | | | | | | | 200 | **200** |
| 5:00 | | | | | | | 200 | **200** |
| 6:00 | | | | | | | 200 | **200** |
| 7:00 | | | | | | | 200 | **200** |
| 8:00 | 100 | | | 50 | | 110 | 200 | **460** |
| 9:00 | | | | | | 110 | 200 | **310** |
| 10:00 | | | | | | 110 | 200 | **310** |
| 11:00 | | | | | | 110 | 200 | **310** |
| 12:00 | | | | | | 110 | 200 | **310** |
| 13:00 | | | | | | 110 | 200 | **310** |
| 14:00 | | | | | | 110 | 200 | **310** |
| 15:00 | | | | | | 110 | 200 | **310** |
| 16:00 | | | | | | 110 | 200 | **310** |
| 17:00 | | | | | | 110 | 200 | **310** |
| 18:00 | | | | | | | 200 | **200** |
| 19:00 | | | | | 115 | | 200 | **315** |
| 20:00 | 100 | 600 | | | 115 | | 200 | **1015** |
| 21:00 | 100 | | | | 115 | | 200 | **415** |
| 22:00 | 100 | | 120 | | | | 200 | **420** |
| 23:00 | 100 | | 120 | | | | 200 | **420** |
| **Total** | **500** | **600** | **240** | **50** | **345** | **1100** | **4800** | **7635** |

4.2. Hybrid system modeling

The primary energy generation and the production of hydrogen are determined by the characteristics of the solar radiation, the PV cells and their coupling to the electrolyzers. As an example, the coupling of ELs to the MPP at the time of maximum daily radiation is shown in Fig. 5 along with the curves of the PV module for different insolation levels.

On using this approach, the relative position and shape of the electrolyzer (EL) curve is determined by the number ($N_{EL}$) and surface ($S_{CEL}$) of EL cells in series connected to the PV modules to achieve the best coupling in each case: for conventional electrolysis this can be achieved with $N_{EL-1} = 18$ and $S_{EL-1} = 3.41\ cm^2$ per module (PV1), as shown in Fig. 5a for the maximum solar radiation, which is close to MPPs for other conditions (Fig. 5b); for ethanol electrolysis these values are much higher, e.g., $N_{EL-2} = 40$ and $S_{EL-2} = 16.1\ cm^2$, and the coupling is worse (Figs. 5a and 5b) because of the different I-V characteristics that make these electrolyzers run at low current densities (J).

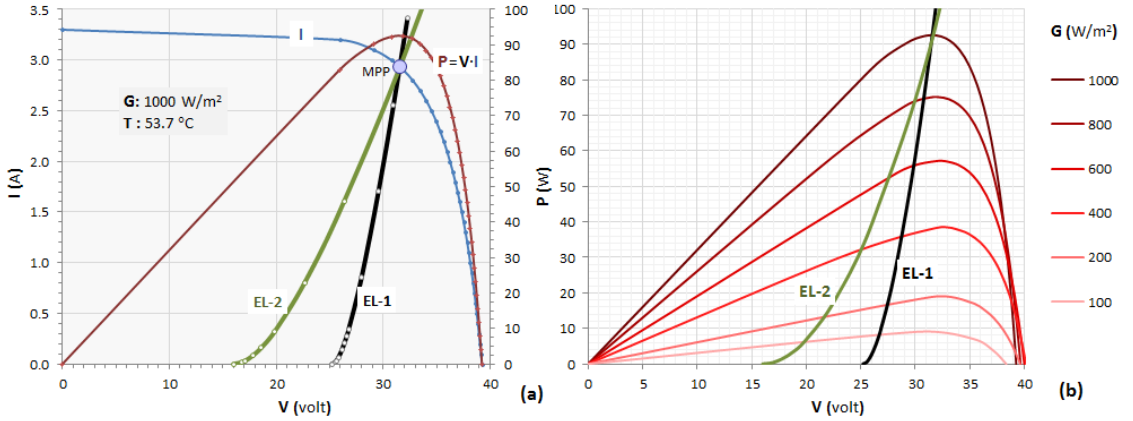


Fig. 5. PV-EL coupling for water electrolysis (EL-1) and ethanol electrolysis (EL-2)

This initial selection of the number and areas of the electrodes allows the following procedure to be proposed to optimize the relative sizing of PV-EL for direct coupling:

1. The electrical intensity of the PV module coupled to the electrolyzer according to the radiation and temperature profiles (eq. 1a & b) is determined by solving equations 2 & 3 simultaneously:

$$I_{PV1,t}(G_t, T_t) = 0 \qquad (4)$$

2. The power generation is then summed and compared to daily consumption in order to estimate the number of modules required using a suitable sizing factor (f):

$$P_{PV1} = \Sigma\,(I \cdot V)_{PV1,t} \qquad (5a) \qquad N_{PV} = f \cdot C / P_{PV1} \qquad (5b)$$

3. The joint generation of the photovoltaic field is reduced with the consumption during the hours of sunlight to impute the excess hourly power destined for the electrolyzer:

$$P_{PV} = \Sigma\, N_{PV} \cdot P_{PV1,t} \qquad (6a) \qquad P_{EL} = \Sigma\, \left| P_{PV,t} - C_t \right| \qquad (6b)$$

4. The total current of the PV modules connected to the electrolyzer is obtained with $P_{EL,t} = (I \cdot V)_{EL,t}$ (eq. 3), together with the electrode area for the maximum (nominal) power:

$$I_{EL,t} = f(P_{EL,t}) \qquad (7a) \qquad S_{CEL} = S_{EL} \cdot (P_{EL}/P_{PV1})_{max} \qquad (7b)$$

5. The hydrogen production is estimated by Faraday´s law ($\Im$ = 96.5 kC/$g_{H2}$), using a net current efficiency ($\eta_{EL}$ = 0.90) to account for small faradic losses and additional energy consumption outside the electrolyzer stack (BOP):

$$Q_H = \Sigma\, N_{EL}\, 3{,}6 \cdot \eta_{EL}\, I_{EL,t} / \Im \quad (8)$$

6. The hydrogen for fuel cells (FCs) is finally taken into account to withstand the power deficits (eq. 9a), with a performance e.g. $\eta_{FC}$ = 0.60 (LHV), as well as the availability of $H_2$ in terms of power differences (SOC):

$$P_{FC} = \Sigma \left| C_t - P_{PV,t} \right| \quad (9a) \qquad SOC = \Sigma \left| Q_{H,t} - P_{FC,t}/\eta_{FC} \right| \quad (9b)$$

The spreadsheet for a simulation scenario with the ethanol electrolyzer (EL-2) over the 24 hour day is shown in more detail in Fig. 6: column B shows the daily consumption of the house (Wh/h) and columns C to G include radiation, temperature and PV module parameters, the current intensity of which is calculated with a solver in columns H-I; columns J to L thus yield the hourly powers, estimate the number of modules with the chosen sizing factor (cells F2 and F3) and obtain the total power and power surplus for electrolysis; a second column pair (M-N) calculates the current to the electrolyzer from which the production of hydrogen (O) is finally obtained for the FC (Q) or for storage (R); the electrode area per cell and total (I2 and I3), as well as the maximum and minimum current densities (L2 and L3), are determined from the extreme hourly average values in columns L and M; finally, the efficiency rate (LHV) and the specific energy consumption of the electrolyzer are calculated in cells R2 and R3 using the outputs from L30 and O30. The solar input amounts to 5 kW/m$^2$day with a PV generation of 0.444 kWh/module; on entering the factor (f = 2.0) the number of modules is 35, the total generation is 15.5 kWh and the power surplus is 12.9 kWh; the total current to EL-2 is 1600 kC/day and the electrode area is 2.036 m$^2$, leading to an operation range of 0.545–1.825 kA/m$^2$; the $H_2$ production is 597 g/day, of which 41.9% is consumed by the FC for home power and the remainder (SOC = 11.6 kWh$_{H2}$) can be used for other applications.

| | A | B | C | D | E | F | G | H | I | J | K | L | M | N | O | P | Q | R |
|---|---|---|---|---|---|---|---|---|---|---|---|---|---|---|---|---|---|---|
| 2 | Enter the consumption profile, | | | | f = | 2.0 | | $S_{CEL}$ (cm$^2$) = | 508.9 | $J_{max}$ (A/cm$^2$): | | 0.1825 | | $\eta_{EL}$ ($\Im$, BOP): | 90% | | | $\eta_e$ = | 154.7% |
| 3 | solar radiation and sizing (f): | | | | $N_{PV}$ = | 35 | | $S_{NEL}$ (m$^2$) = | 2.0356 | $J_{min}$ (A/cm$^2$): | | 0.0545 | | $\eta_{FC}$ (LHV): | 60% | | Ce (kWh/kg$_{H2}$)= | 21.7 |
| 5 | t (h/day) | C (W) | G (W/m$^2$) | T (K) | a | $I_0$ | $I_{SC}$ | $I_{PV1}$ (A) | f(I)=0 | $P_{PV1}$ (W) | $P_{PV}$ (W) | $P_{EL}$ (W) | $I_{EL}$ (A) | f($P,I_{EL}$)=0 | $Q_H$ (g/h) | | $P_{FC}$ (W) | SOC ($W_{H2,LHV}$) |
| 6 | 0 | 200 | 0 | 278.0 | 3.2018 | 1.481E-06 | 0.0000 | search | objective | 0.00 | 0.0 | 0.0 | search | objective | 0.00 | ## | 200.0 | -333.3 |
| 7 | 1 | 200 | 0 | 278.0 | 3.2018 | 1.481E-06 | 0.0000 | | | 0.00 | 0.0 | 0.0 | | | 0.00 | ## | 200.0 | -333.3 |
| 8 | 2 | 200 | 0 | 278.0 | 3.2018 | 1.481E-06 | 0.0000 | | | 0.00 | 0.0 | 0.0 | | | 0.00 | ## | 200.0 | -333.3 |
| 9 | 3 | 200 | 0 | 278.0 | 3.2018 | 1.481E-06 | 0.0000 | | | 0.00 | 0.0 | 0.0 | | | 0.00 | ## | 200.0 | -333.3 |
| 10 | 4 | 200 | 0 | 278.0 | 3.2018 | 1.481E-06 | 0.0000 | | | 0.00 | 0.0 | 0.0 | | | 0.00 | ## | 200.0 | -333.3 |
| 11 | 5 | 200 | 0 | 278.0 | 3.2018 | 1.481E-06 | 0.0000 | | | 0.00 | 0.0 | 0.0 | | | 0.00 | ## | 200.0 | -333.3 |
| 12 | 6 | 200 | 0 | 278.0 | 3.2018 | 1.481E-06 | 0.0000 | | | 0.00 | 0.0 | 0.0 | | | 0.00 | ## | 200.0 | -333.3 |
| 13 | 7 | 200 | 0 | 278.0 | 3.2018 | 1.481E-06 | 0.0000 | | | 0.00 | 0.0 | 0.0 | | | 0.00 | ## | 200.0 | -333.3 |
| 14 | 8 | 460 | 0 | 278.0 | 3.2018 | 1.481E-06 | 0.0000 | | | 0.00 | 0.0 | 0.0 | | | 0.00 | ## | 460.0 | -766.7 |
| 15 | 9 | 310 | 95 | 282.7 | 3.2554 | 2.484E-06 | 0.3120 | 0.311 | 0.00 | 6.15 | 215.3 | 0.0 | 0.00 | 0.0 | 0.00 | ## | 94.7 | -157.8 |
| 16 | 10 | 310 | 345 | 294.8 | 3.3957 | 8.390E-06 | 1.1296 | 1.120 | 0.00 | 27.11 | 948.8 | 638.8 | 27.74 | 0.0 | 37.25 | ## | 0.0 | 1249.9 |
| 17 | 11 | 310 | 655 | 309.9 | 3.5692 | 2.993E-05 | 2.1417 | 2.072 | 0.00 | 58.55 | 2049.3 | 1739.3 | 62.43 | 0.0 | 83.84 | ## | 0.0 | 2813.3 |
| 18 | 12 | 310 | 905 | 322.1 | 3.7096 | 7.171E-05 | 2.9617 | 2.728 | 0.00 | 83.97 | 2939.0 | 2629.0 | 85.63 | 0.0 | 115.00 | ## | 0.0 | 3858.7 |
| 19 | 13 | 310 | 1000 | 326.7 | 3.7632 | 9.703E-05 | 3.2752 | 2.934 | 0.00 | 92.59 | 3240.7 | 2930.7 | 92.87 | 0.0 | 124.73 | ## | 0.0 | 4185.2 |
| 20 | 14 | 310 | 905 | 322.1 | 3.7096 | 7.171E-05 | 2.9617 | 2.728 | 0.00 | 83.97 | 2939.0 | 2629.0 | 85.63 | 0.0 | 115.00 | ## | 0.0 | 3858.7 |
| 21 | 15 | 310 | 655 | 309.9 | 3.5692 | 2.993E-05 | 2.1416 | 2.072 | 0.00 | 58.55 | 2049.2 | 1739.2 | 62.43 | 0.0 | 83.84 | ## | 0.0 | 2813.3 |
| 22 | 16 | 310 | 345 | 294.8 | 3.3957 | 8.389E-06 | 1.1295 | 1.120 | 0.00 | 27.10 | 948.5 | 638.5 | 27.74 | 0.0 | 37.25 | ## | 0.0 | 1249.9 |
| 23 | 17 | 310 | 95 | 282.7 | 3.2554 | 2.484E-06 | 0.3120 | 0.311 | 0.00 | 6.14 | 214.8 | 0.0 | 0.00 | 0.0 | 0.00 | ## | 95.2 | -158.6 |
| 24 | 18 | 200 | 0 | 278.0 | 3.2018 | 1.481E-06 | 0.0000 | | | 0.00 | 0.0 | 0.0 | | | 0.00 | ## | 200.0 | -333.3 |
| 25 | 19 | 315 | 0 | 278.0 | 3.2018 | 1.481E-06 | 0.0000 | | | 0.00 | 0.0 | 0.0 | | | 0.00 | ## | 315.0 | -525.0 |
| 26 | 20 | 1015 | 0 | 278.0 | 3.2018 | 1.481E-06 | 0.0000 | | | 0.00 | 0.0 | 0.0 | | | 0.00 | ## | 1015.0 | -1691.7 |
| 27 | 21 | 415 | 0 | 278.0 | 3.2018 | 1.481E-06 | 0.0000 | | | 0.00 | 0.0 | 0.0 | | | 0.00 | ## | 415.0 | -691.7 |
| 28 | 22 | 420 | 0 | 278.0 | 3.2018 | 1.481E-06 | 0.0000 | | | 0.00 | 0.0 | 0.0 | | | 0.00 | ## | 420.0 | -700.0 |
| 29 | 23 | 420 | 0 | 278.0 | 3.2018 | 1.481E-06 | 0.0000 | | | 0.00 | 0.0 | 0.0 | | | 0.00 | ## | 420.0 | -700.0 |
| 30 | **Total:** | **7635** | **5000** | | | $R_{s,r}$ = | -0.2829 | | | **444.13** | **15544.6** | **12944.5** | 1600.073 | kC/d | **596.92** | | **5034.9** | **11637.5** |

Fig. 6. Spreadsheet for calculating the hybrid system daily profiles

## 5. Results from simulations, cost analysis and discussion

The optimum design of the hybrid systems requires the identification of the size and configuration of the solar field and the electrolyzer in order to minimize the total costs of the installations while ensuring the load coverage [i.e., SOC (Wh/d) $\geq 0$], in addition to other limitations on the operating conditions of the equipment (e.g., $J_{min}$ and $J_{max}$).

The spreadsheets of the cases studied allow a detailed appreciation of the data sets, the simulated variables and the results obtained. This allows the design to be discussed from a techno-economic point of view and to obtain conclusions regarding modeling, simulation and optimization of hybrid hydrogen and solar energy system coupling.

The power outputs from the modules ($P_{FV}$), the power loads of the house (C), the inputs to the electrolyzer ($P_{EL}$), the hydrogen produced by the EL or utilized in FC (SOC), the FC generation ($P_{FC}$), and the cumulative state-of-charge of the storage system throughout the day ($Wh_{H2}$/day) are shown in Fig. 7 according to the spreadsheets (Fig. 6), the main results of which are summarized in Table 3.

Both systems are simulated to cover the power loads of the house while producing and storing almost the same amount of $H_2$ (ca. 11.6 kWh/d, as shown in Fig. 7 and Table 3), but their operation is quite different in terms of primary energy requirements, current densities and size of the electrolyzers. Therefore, an economic estimate of the systems based on the equipment size, the specific costs of the components and consumption of reagents was obtained as depicted in Table 4.

The price of PV modules is taken as 1.3 €/$W_p$ with a lifetime of 25 years and O&M of 2% per year [32], the EL is purchased at 4075 €/$Nm^3_{H2}h^{-1}$ and this may be scaled by an exponent of 0.7 based on electrode area with a lifetime of 20 years and O&M of 1%, the deposit for 15 days storage ($H_2$-FC) at 38 €/$Nm^3$ in 20 years and 0.5% [33], the cost of FC 3000 €/kW in 10 years and 2.5% [34] and the consumption of EtOH at 0.50 €/l [35]; finally, the hydrogen surplus is assumed to be sold in the energy market at 4.0 €/$kg_{H2}$.

It can be seen that the electrochemical reforming system with ethanol has an initial investment and annual costs higher than conventional electrolysis, because the former requires a much larger surface area of electrodes, as well as consumption of alcohol; however, the conventional process requires a much higher sizing of the solar field as a consequence of its greater voltages (1.45–1.75 V) when compared to the organic based process (0.58–0.79 V), which has a consumption and energy efficiency that is much more favorable (155% vs. 67%). The current densities can be maintained in both cases within the limits for their proper operation and both systems allow self-sufficiency in electrical energy in the home as well as a surplus of 0.35 $kg_{H2}$/d, which would provide benefits of ca. 500 €/a.

As the direct coupling design is focused on a system in which the PV output is fed to the EL or home demands at different rates, it also requires real-time control of parallel wiring interconnections to keep the PV at its operation points when it is hooked up to the loads. Also, under variable loads, a minimum input current must be guaranteed to accomplish with quality standards, whereas below a minimum current the EL should be switched off and the rate of change of the supply current is kept bounded to reduce internal wear. Finally, the power loss was not considered as the excess power produced by the PV array is never more than the nominal power input of the EL.

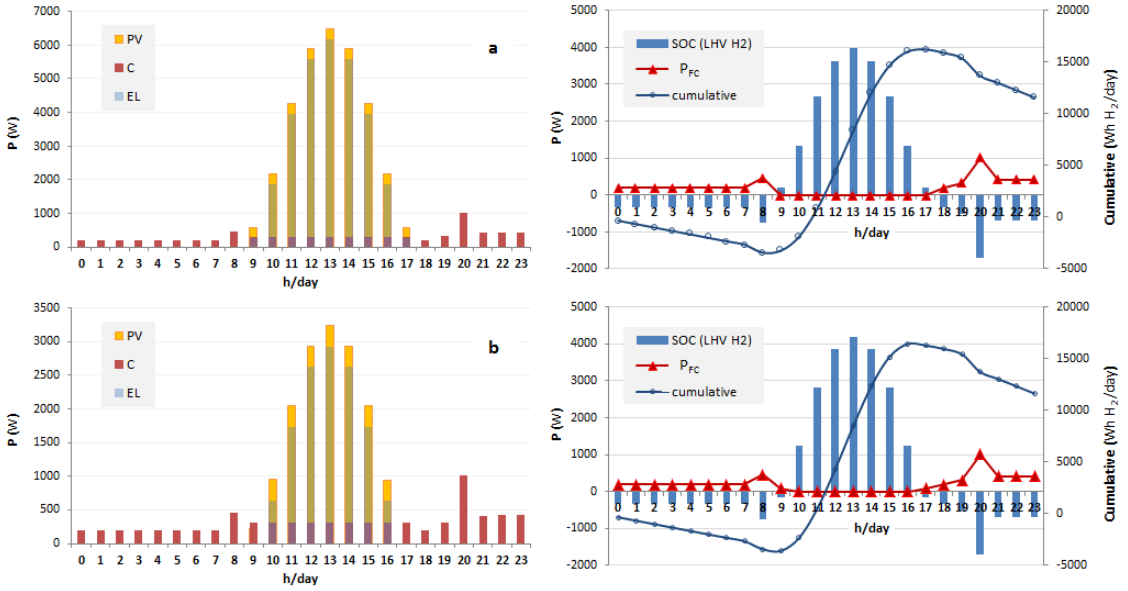


Fig. 7. Simulation results for coupling the water electrolyzer (a) and ethanol electrolyzer (b)

Table 3. Simulation results for coupling the water electrolyzer (a) and ethanol electrolyzer (b)

| **Parameter** | **(units)** | **a** | **b** |
|---|---|---|---|
| Power generation (per PV module), $P_{PV1} = \Sigma P_{PV1,t}(G_t)$ | (Wh/d) | 461.5 | 444.1 |
| Sizing factor, f | | 4.2 | 2.0 |
| Number of PV modules, $N_{PV} = f \cdot C/P_{PV1}$ | | 70 | 35 |
| Power generation (PV total), $P_{PV} = \Sigma N_{PV} \cdot P_{PV1,t}$ | (Wh/d) | 32305 | 15545 |
| Power to electrolyzer, $P_{EL} = \Sigma \lvert P_{PV,t} - C_t \rvert$ | (Wh/d) | 29515 | 12945 |
| Input current to electrolyzer $I_{EL} = \Sigma f(P_{EL,t})$ | (kC/d) | 3490.4 | 1600.1 |
| Electrode area (total), $S_{NEL} = N_{EL} \cdot S_{CEL}$ | ($m^2$) | 0.4095 | 2.0356 |
| Minimum current density, $J_{min} = I_{EL,min}/S_{CEL}$ | ($kA/m^2$) | 0.430 | 0.545 |
| Maximum current density, $J_{max} = I_{EL,max}/S_{CEL}$ | ($kA/m^2$) | 8.597 | 1.825 |
| Hydrogen production, $Q_H = \Sigma N_{EL} \cdot 3{,}6 \cdot \eta_{EL} I_{EL,t}/96{,}5$ | (g/d) | 586.0 | 596.9 |
| Specific energy yield, $C_e = P_{EL}/Q_H$ | ($kWh/kg_{H2}$) | 50.4 | 21.7 |
| Fuel cell power, $P_{FC} = \Sigma \lvert C_t - P_{PV,t} \rvert$ | (Wh/d) | 4845.0 | 5034.9 |
| Cumulative energy stored, SOC | ($Wh_{H2,LHV}$) | 11586 | 11638 |

Table 4. Cost analysis of the hybrid systems with conventional (a) and ethanol (b) electrolyzers

| **Cost items (units, u)** | | **Size units (u)** | | **Unit cost** | **Investment costs (€)** | | **Annual costs (€/a)** | |
|---|---|---|---|---|---|---|---|---|
| | | **a** | **b** | **(€/u)** | **a** | **b** | **a** | **b** |
| PV modules | ($W_p$) | 6481.5 | 3240.7 | 1.29 | 8354.9 | 4177.5 | 501.3 | 250.6 |
| Electrolyzer | ($m^2_{NEL}$) | 0.4095 | 2.0356 | 10072 | 5391.1 | 16565.0 | 323.5 | 993.9 |
| Fuel cell | (kW) | 1.015 | 1.015 | 3000 | 3045.0 | 3045.0 | 380.6 | 380.6 |
| $H_2$ deposit | ($Nm^3$) | 40.4 | 42.0 | 38 | 1535.4 | 1595.4 | 84.4 | 87.7 |
| Ethanol | (l/d) | 0 | 2.90 | 0.50 | 0 | - | 0 | 529.3 |
| **Total costs** | | | | | **18326** | **25383** | **1290** | **2242** |

Sensitivity analysis.- Three simulation cases for coupling the organic electrolyzers with different I-V curves converging on $G_m$ (MPP), but having different numbers and areas of electrodes, are presented for an initial parametric study of the main variables (Fig. 8a). The sizing factor of the PV array was scaled in all cases to produce similar hydrogen surpluses (SOC variation is 11.5–11.7 $kWh_{H2}$/day) in order to make them comparable. Three new cases in which the number of EL cells with the same area were modified are simulated in Fig. 8b and these give curves that intersect PV lines at points apart from $G_m$ (MPP). As expected, increases in EL sizes in series reduces the PV size as the coupling throughout the G (MPP) space is improved (i.e., the EL runs at lower intensity with lower energy utilization), but these gains are quite limited and also occur at the expense of somewhat larger electrolyzers. As indicated above, the sizing factors for the solar field have to be modified in each case to achieve a similar SOC value. However, if this factor had been set as in case 0 (f = 2.0) to keep the number of solar modules approximately constant, the results in case 1 represent savings in electrode area and a lower $H_2$ surplus (0.77 $m^2$, 7.1 kWh/d), whereas case 2 follows the opposite trend (5.4 $m^2$, 15.8 kWh/d). The energy efficiency and the $J_{max}$ of the electrolyzer are not modified, even if the $J_{min}$ is (1.102 and 0.251 $kA/m^2$).

The results summarized below clearly indicate that as `EL coupling´ improves, the required solar field is reduced, but in turn the size of the electrolyzer becomes much larger. Therefore, in economic terms it would not be particularly advantageous to operate near to the `maximum power points' (which require lower current densities), even if they give rise to more favorable specific energy consumptions.

On the basis of the above discussion, it can be concluded that the most important criterion for system optimization is the reduction of the electrolyzer size as opposed to primary energy transfer from solar modules, due to the cost of the components and the voltage characteristics of the organic electrolyzer. Thus, case 0 is considered as an optimal configuration bearing in mind the operation dynamics, the efficiency of the energy conversion, the sizes of the components and the resulting costs.

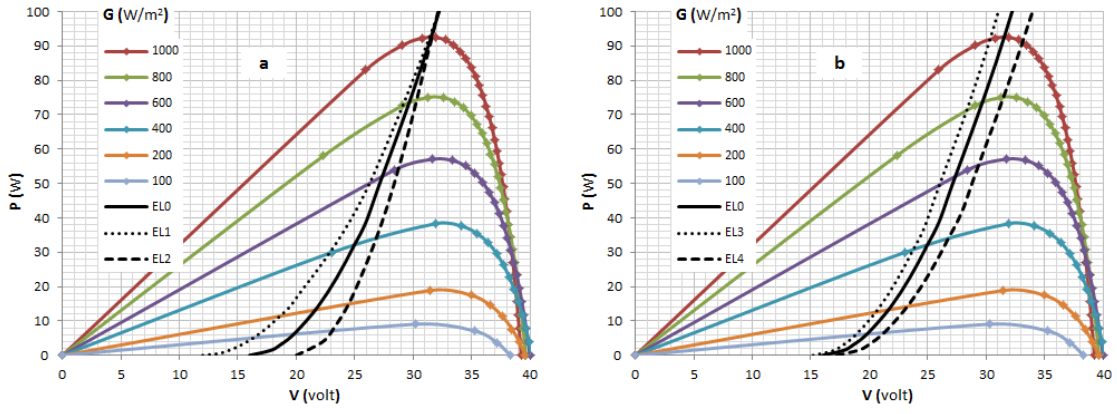


| Case | $N_{PV}$ | $S_{NEL}$ ($m^2$) | J ($kA/m^2$) | $C_e$ ($kWh/kg_{H2}$) | $C_a$ (€/a) |
|---|---|---|---|---|---|
| EL0 | 35 | 2.04 | 0.545 - 1.825 | 21.7 | 2242 |
| EL1 | 45 | 0.98 | 1.175 - 3.724 | 28.2 | 1929 |
| EL2 | 29 | 4.48 | 0.238 - 0.840 | 17.8 | 2930 |
| EL3 | 36 | 1.99 | 0.541 - 1.886 | 21.8 | 2231 |
| EL4 | 34 | 2.12 | 0.552 - 1.707 | 21.4 | 2258 |

Fig. 8. Simulation cases for coupling the ethanol reforming electrolyzer to the PV solar modules

Furthermore, perhaps the most interesting issue for parametric analysis is to anticipate the `breakeven´ values of the operating and cost variables of the organic electrolyzers that match them to conventional systems and to ensure that their hybridization with a solar (PV) source is cost-effective compared to other energy solutions.

For this analysis the water electrolyzer (a) can be compared to the ethanol reforming electrolyzer (b) using the base configuration to couple the hybrid system (i.e., case 0), which means the sizes of units as shown in Table 4. The unit costs of the components are then simulated so that the annual costs of both systems are equivalent: the critical components are the PV and EL only as the FC and $H_2$ deposit have in practice the same dimensions and costs. The composition of the costs for the different scenarios are shown in Fig. 9: (a) corresponds to hybridization of a conventional EL, which amounts to 1290 €/a with 39% of costs due to PVs, 25% EL, 29% FC and 7% $H_2$ deposit; (b) is the organic EL (2242 €/a) with 11% of the cost due to PVs, 44% EL, 17% FC, 4% $H_2$ deposit and 24% from EtOH consumption; finally, (c) and (d) are two cases in which the costs of organic ELs are matched to the costs of a conventional EL. Thus, the simulations showed that the unit cost of the organic electrolyzer should drop to 420 €/$m^2$ (i.e., a 96% cost reduction), which seems unlikely (case c). This is due to the lower current densities of the EL but also to the EtOH consumed in the electro-reforming process. If an inexpensive organic substrate could be used instead (case d), the cost reduction of the EL should be only 43% to match the same annual costs as using conventional water electrolysis (this would hopefully promote the use of residual biomass products, which in turn would provide both energy and environmental advantages).

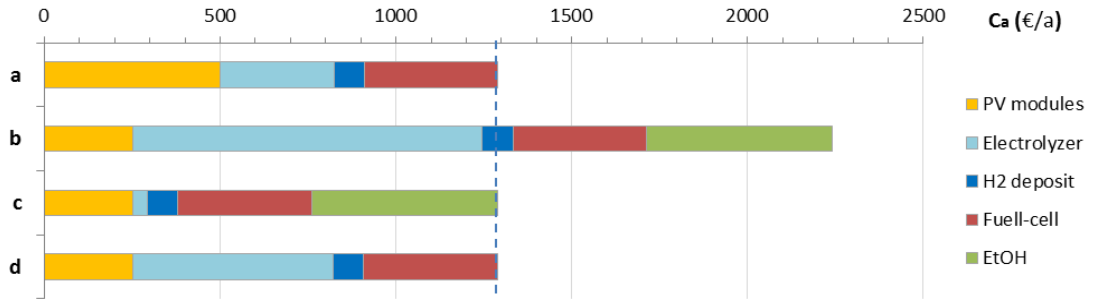


Fig. 9. Composition of annual costs for different scenarios (a, b, c, d)

It should also be noted that the price of PV modules was taken on the basis of the cost reduction rates of these technologies, which are now quite favorable. Therefore, this factor hardly compensates for the reduction of the solar field that is achieved with the implementation of the hybrid energy systems. In this sense, the electricity supplied by hybrid systems such as the ones described in this paper costs 0.28 €/kWh after deducting $H_2$ sales (i.e., approx. the same as current power prices for home consumers in Spain, which include taxes, levies and other regulated costs due to grid connection). However, the hybrid system has the merit of being autonomous and the $H_2$ has the capacity for seasonal energy storage, thus avoiding electrification constraints in off-grid locations as well as limitations of batteries, which are only capable of short-term power storage; this was assessed in recent communications where authors show that hydrogen is the most effective carrier for storage of stochastic renewable energy in the long-term, as the costs of electric accumulators increase much faster than the costs of the hydrogen systems when the time of energy storage rises [36, 37].

These results indicate that although the technology is still in early development stages and costs are very uncertain, the integrated systems built with PV and $H_2$ can play an effective role in implementing a distributed energy supply in applications that require seasonal storage with compact, long life and low maintenance devices.

The hydrogen storage sub-system is economically beneficial if its lifecycle cost is less than the costs of additional PV cells, the short-term storage (e.g. batteries) or a fuel generator (or both), that would be necessary if there was no hydrogen storage; this was also assessed in another study showing that it becomes economically-viable at given solar ratios (latitudes) for round-trip efficiencies lower than what are already achievable with present-day technology [38].

Thus, the use of hydrogen eliminates the need for high number of solar cells and battery units with low life span, although there may also be an additional small-sized storage unit consisting of battery, ultra-capacitor, etc. -as a buffer of fast variations in load demands- considering the relatively slow response of FC technology [39]; this system uses the FC as a base power device and the battery as a peak-load device, however, we have considered that FCs are designed to operate in this fashion (i.e., they can meet the fast demand ramp rates observed in residences).

Hybrid systems with direct connection of PV and batteries to smooth the power supply to EL have also been analyzed to operate in better operation points and increase the full load hours (due to discrete EL sizes and minimum energy requirements); however, one key finding is that the use of batteries is currently more expensive than building more electrolyzer capacity [40].

Finally, the safety threats of the hybrid systems, especially the hydrogen storage tanks, should not be ignored for a proper deployment of the technology in residential applications.

## 6. Concluding remarks

It can be concluded that the integration of hydrogen and solar energy technologies by the hybridization of photovoltaic panels coupled to hydrogen generators is a viable option – with reasonable capital and operating costs – to satisfy energy requirements in a location that is isolated from the electricity grid.

The main advantage of PV-$H_2$ hybrid systems for an independent home grid, when compared with a separate PV array, is the possibility of surplus energy storage by means of an EL, which transforms the electricity into $H_2$ that can be used in FCs.

The study presented here concerns a novel model to analyze and design PV-$H_2$ systems that considers the weather data and performs effective energy balances to assess the hybrid system by the load requirements, the levels of energy stored and the resulting costs. A good knowledge of PV & EL characteristics allows the optimization of stand-alone energy systems that fulfill power needs in full operation over time.

Two electrolytic systems were analyzed (conventional water and ethanol reforming) and this represents another contribution of this work in the search for the best trade-off between the minimum sizes and voltages of the electrolyzers.

The results show that as PV-EL coupling is improved, the solar field is reduced while the size of EL becomes much larger; therefore, it would not be particularly advantageous to operate near to the maximum power points (which require lower current densities), even if they imply more favorable specific energy consumption.

Organic electrolysis has the advantage of significantly lowering the primary energy requirements, although it should be accompanied by developments to improve current

densities at the electrodes and reduce the costs of the electrolyzer. The use of other organic substrates that allow for cheaper reagent costs should also be investigated.

The breakeven prices were determined for the organic electrolyzers that match them to conventional systems and ensure that hybridization with PV sources is cost-effective compared to non-autonomous energy solutions.

**Acknowledgement**

A. B. Calcerrada would like to thank to the `Junta de Comunidades de Castilla-La Mancha, JCCM)´ and the `European Social Found´ for financial support.

## References

[1] Alanne K, Cao S. Zero-energy hydrogen economy (ZEH2E) for buildings and communities including personal mobility. Renewable and Sustainable Energy Reviews 2017;71:697-711.

[2] Barbir F. PEM electrolysis for production of hydrogen from RES. Solar Energy 2005;78:661-69.

[3] Deshmukh SS, Boehm RF. Review of modeling details related to renewably powered hydrogen systems. Renewable and Sustainable Energy Reviews 2008;12:2301-30.

[4] Erdinc O, Uzunoglu M. Optimum design of hybrid renewable energy systems: overview of different approaches. Renewable and Sustainable Energy Reviews 2012;16:1412-25.

[5] Maclay JD, Brouwer J, Samuelsen GS. Experimental results for hybrid energy storage systems coupled to PV generation in residential applications. Int J Hydrogen Energy 2011;36:12130-40.

[6] Andrews J, Shabani B. Dimensionless analysis of the global techno-economic feasibility of solar-$H_2$ systems for constant year-round power supply. Int J Hydrogen Energy 2012;37:6-18.

[7] Gray E MacA, Webb CJ, Andrews J, Shabani B, Tsai PJ, Chan SLI. Hydrogen storage for off-grid power supply. Int J Hydrogen Energy 2011;36:654-63.

[8] Kelly NA, Gibson TL, Ouwerkerk DB. Generation of high-pressure hydrogen for FC electric vehicles using PV-powered water electrolysis. . Int J Hydrogen Energy 2011;36:15803-25.

[9] Kelly NA. The coupling factor: a new metric for determining and controlling the efficiency of solar photovoltaic power utilization. Int J Hydrogen Energy 2013;38:2079-94.

[10] Bajpai P, Dash V. Hybrid renewable energy systems for power generation in stand-alone applications: a review. Renewable and Sustainable Energy Reviews 2012;16:2926-39.

[11] Escobar B, Hernández J, Barbosa R, Verde-Gómez Y. Analytical model as a tool for the sizing of a hydrogen production system based on renewable energy: the Mexican Caribbean as a case of study. Int J Hydrogen Energy 2013;38:12562-69.

[12] Yunez-Cano A, González-Huerta RG, Tufiño-Velázquez M, Barbosa R, Escobar B. Solar-hydrogen hybrid system integrated to a sustainable house in Mexico. Int J Hydrogen Energy 2016;41:19539-45.

[13] Alanne K, Cao S. Zero-energy hydrogen economy (ZEH2E) for buildings and communities including personal mobility. Renewable and Sustainable Energy Reviews 2017;71:697-711.

[14] Atlam O, Barbir F, Bezmalinovic D. A method for optimal sizing of an electrolyzer directly connected to a PV module. Int J Hydrogen Energy 2011;36:7012-18.

[15] Maroufmashat A, Sayedin F, Khavas SS. An imperialist competitive algorithm approach for multi-objective optimization of direct coupling PV-EL. Int J Hydrogen Energy 2014;39:18743-57.

[16] Migoni G, Rullo P, Bergero F, Kofman E. Efficient simulation of Hybrid Renewable Energy Systems. Int J Hydrogen Energy 2016;41:13934-49.

[17] Khalilnejad A, Abbaspour A, Sarwat AI. Multi-level optimization approach for directly coupled photovoltaic-electrolyser system. Int J Hydrogen Energy 2016;41:11884-94.

[18] Eltawil MA, Zhao Z. MPPT techniques for photovoltaic applications. Renewable and Sustainable Energy Reviews 2013;25:793-813.

[19] Su Z, Ding S, Gan Z, Yang X. Optimization and sensitivity analysis of a photovoltaic-electrolyser direct-coupling system in Beijing. Int J Hydrogen Energy 2014;39:72002-15.

[20] Yang Z, Zhang G, Lin B. Performance evaluation and optimum analysis of a photovoltaic-driven electrolyzer system for hydrogen production. Int J Hydrogen Energy 2015;40:3170-79.

[21] Take T, Tsurutani K, Umeda M. Hydrogen production by methanol–water solution electrolysis. J Power Sources 2007;164:9-16.

[22] Tebibel H, Khellaf A, Menia S, Nouicer I. Design, modelling and optimal power and hydrogen management strategy of an off grid PV system for hydrogen production using methanol electrolysis. Int J Hydrogen Energy 2017;42:14950-67.

[23] Sapountzi FM, Tsampas MN, Fredriksson HOA, Gracia JM, Niemantsverdriet JW. Hydrogen from electrochemical reforming of C1-C3 alcohols using proton conducting membranes. Int J Hydrogen Energy 2017;42:10762-74.

[24] Rezaee Jordehi A. Parameter estimation of solar photovoltaic (PV) cells: a review. Renewable and Sustainable Energy Reviews 2016;61:354-71.

[25] Duffie JA, Beckmann WA. Solar engineering of thermal processes. 3rd ed. NY: Wiley; 2006.

[26] García-Valverde R, Espinosa N, Urbina A. Optimized method for photovoltaic-water electrolyser direct coupling. Int J Hydrogen Energy 2011;36:10574-86.

[27] Townsend TU. A method for estimating the long-term performance of direct-coupled photovoltaic systems [MSc dissertation]: Mechanical Engineering, University of Wisconsin-Madison; 1989.

[28] Shen M, Bennett N, Ding Y, Scott K. A concise model for evaluating water electrolysis. Int J Hydrogen Energy 2011;36:14335-41.

[29] Millet P et al. PEM water electrolyzers: from electrocatalysis to stack development. Int J Hydrogen Energy 2010;35:5043-52.

[30] Caravaca A, Sapountzi FM, De Lucas-Consuegra A, Molina-Mora C, Dorado F, Valverde JL. Electrochemical reforming of ethanol-water solutions for pure $H_2$ production in a PEM electrolysis cell. Int J Hydrogen Energy 2012;37:9504-13.

[31] De Lucas-Consuegra A, De la Osa AR, Calcerrada AB, Linares JJ, Horwat D. A novel sputtered Pd mesh architecture as an advanced electrocatalyst for highly efficient hydrogen production. J Power Sources 2016;321:248-56.

[32] Autosolar. Paneles solares. https://autosolar.es/panel-solar/panel-solar-monocristalino/

[33] Zoulias EI, Lymberopoulos N. Techno-economic analysis of the integration of $H_2$ energy technologies in RE-based stand-alone power systems. Renewable Energy 2007;32:680-96.

[34] Erdinc O, Uzunoglu M. A new perspective in optimum sizing of HRES: consideration of component performance degradation issue. Int J Hydrogen Energy 2010;35:5043-52.

[35] García MJM. Máximos históricos para la producción de bio-etanol. Agrodigital (2015).

[36] Marchenko OV, Solomin SV. The future energy: Hydrogen versus electricity. Int J Hydrogen Energy 2015;40:3801-05.

[37] Abdin Z, Webb CJ, Gray E. Solar hydrogen hybrid energy systems for off-grid electricity supply: A critical review. Renewable and Sustainable Energy Reviews 2015;52:1791-1808.

[38] Andrews J, Shabani B. Dimensionless analysis of the global techno-economic feasibility of solar-$H_2$ systems for constant year-round power supply. Int J Hydrogen Energy 2012;37:6-18.

[39] Nasri S, Ben Slama S, Yahyaoui I, Zafar B, Cherif A. Autonomous hybrid system and coordinated intelligent management approach in power system operation and control using hydrogen storage. Int J Hydrogen Energy 2017;42:9511-23.

[40] Gillessen B, Heinrichs HU, Stenzel P, Linssen J. Hybridization strategies of power-to-gas systems and battery storage using renewable energy. Int J Hydrogen Energy 2017;42:13554-67.